frontiers | Frontiers in Earth Science

TYPE Original Research
PUBLISHED 04 January 2023
DOI 10.3389/feart.2022.1092686

OPEN ACCESS

EDITED BY
Maodu Yan,
Institute of Tibetan Plateau Research(CAS), China

REVIEWED BY
Jinbo Zan,
Institute of Tibetan Plateau Research (CAS), China
Wei Yuan,
Tongji University, China
Zhaojie Yu,
Institute of Oceanology (CAS), China

*CORRESPONDENCE
Jishang Xu,
jishangxu@ouc.edu.cn

SPECIALTY SECTION
This article was submitted to Geomagnetism and Paleomagnetism, a section of the journal Frontiers in Earth Science

RECEIVED 08 November 2022
ACCEPTED 13 December 2022
PUBLISHED 04 January 2023

CITATION
Wang G, Xu J, Jiang Z, Li G, Zhang Y, Zhang W and Liu Y (2023), Precipitation variations of western equatorial pacific during glacial–interglacial cycles since MIS8: Evidence from multi–proxies of abyssal sediment.
Front. Earth Sci. 10:1092686.
doi: 10.3389/feart.2022.1092686

Precipitation variations of western equatorial pacific during glacial–interglacial cycles since MIS8: Evidence from multi–proxies of abyssal sediment

Genmin Wang[1], Jishang Xu[1,2]*, Zhaoxia Jiang[1,2], Guangxue Li[1,2], Yang Zhang[1], Wenchao Zhang[1] and Yong Liu[1]

[1]Key Laboratory of Submarine Geosciences and Prospecting Techniques (MOE), Frontiers Science Center for Deep Ocean Multispheres and Earth System, Engineering Research Center of Marine Petroleum Development and Security Safeguard (MOE), College of Marine Geosciences, Ocean University of China, Qingdao, China, [2]Qingdao National Laboratory for Marine Science and Technology, Qingdao, China

As an important global water vapor source, the Western Pacific warm pool (WPWP) influences precipitation changes in middle and low latitudes. The low-latitude water cycle is a key climate parameter at different time scales, as it contributes to various feedback processes. However, at present, indicators of precipitation variability in the equatorial western Pacific are limited. In this work, we used the sedimentary record of the southern margin of the WPWP to study the precipitation variability over the western equatorial Pacific since MIS8. The age framework based on plankton-foraminifera $\delta^{18}O$ was used to analyze changes in geochemical elements, clay minerals, and magnetic parameters of a marine sediment core H10. As new precipitation records, our precipitation records (TiO_2, χ, and SIRM concentration without carbonate base) are closely related to monsoon and Intertropical Convergence Zone and generally in inverse phase with the oxygen isotope records of stalagmites from caves in China. A spectral analysis showed an obvious precession period. The southern margin of the WPWP water cycle is closely related to the East Asian monsoon in the last four climate cycles, and is influenced by both high and low latitudes.

KEYWORDS

western pacific warm pool, precipitation variability, intertropical convergence zone (ICTZ), environmental magnetism, geochemical elements

1 Introduction

The low-latitude tropical Pacific Ocean is the primary source of global ocean heat and water vapor in the mid- and low-latitude regions, owing to its high temperature and strong atmosphere–ocean interactions. The tropical Pacific variations induce global variations in atmospheric circulation and precipitation (Yan et al., 1992; Wang and Mehta, 2008). The scale, temperature, and precipitation of the tropical Pacific are affected by several factors, such as the Intertropical Convergence Zone (ITCZ), solar insolation, and volcanic activities (Yan et al., 1992; Webster, 1994; Shang et al., 2022). Location and intensity variations of the ITCZ significantly impact tropical precipitation, while the monsoons are the manifestations of the seasonal migration of the ITCZ (Gadgil, 2003). On the seasonal timescale, precipitation along the Pacific coast of the western Pacific is determined *via* the relationship between the location of the Asian–Australian monsoon (AAM) and the ITCZ (Tachikawa et al., 2011). As part of the Asian monsoon, the Australian monsoon system synchronically changes with the Asian monsoon in modern climates: the dry Australian winter monsoon is synchronized with the wet East Asian summer, and *vice versa* (Trenberth et al., 2000).

Studies on the monsoon variations and paleo-precipitation in the tropical western Pacific region reported a close relationship among the hydrology, monsoon system, and solar insolation (Tachikawa et al., 2011; Fraser et al., 2014; Dang et al., 2015). However, complex regional differences were revealed by various sedimentary records (Tachikawa et al., 2011; Wu et al., 2013; Fraser et al., 2014; Rao et al., 2015). Present controversies over the Asian summer monsoon (ASM) are related to its periodic evolution and driving mechanism. The ASM is mainly controlled by variations in solar insolation (Yuan et al., 2004); however, previous findings suggested that changes in the global ice volume are a critical influencing factor (Ding et al., 1995). Recent studies emphasized the influence of orbital forcing (especially precession forcing) on low-latitude tropical monsoons and hydrology (Kissel et al., 2010; Fraser et al., 2014; Cheng et al., 2017). However, better understanding of the paleo-precipitation and monsoon intensity changes in the tropical western Pacific is hampered by the limited records of precipitation and monsoon indicators over long-time scales.

In recent years, environmental magnetism has been widely used as an alternative proxy for paleoenvironmental and paleoclimatic variations (Verosub and Roberts, 1995; Yang et al., 2008). One study has demonstrated a definite relationship between magnetic susceptibility and temperature, monsoon intensity, and precipitation (Han et al., 1996). The magnetic susceptibility of Chinese loess is one of the most reliable indicators for recording the dynamic evolution of the East Asian summer monsoon (EASM) (An et al., 1990; Hao et al., 2012). Environmental magnetic methods are also widely applied in the tropical western Pacific region. For example, as a magnetic mineral grain size indicator, the ratio of anhysteretic remanent magnetization susceptibility (χ_{ARM}) to magnetic susceptibility has been used to reflect changes in the upper waterbody of the West Philippine Sea (Meng et al., 2009). The grain size characteristics of environmental magnetism can also indicate the East Asian monsoon (Hou et al., 2020). Based on the variations in particle size and magnetic susceptibility of minerals in the South China Sea sediments, Kissel et al. (2010) studied the relationship between precipitation, the East Asian monsoon, and deep-sea circulation. Therefore, magnetic parameters can reveal important information on paleoclimatic changes. In this study, the magnetic parameters of the marine sediment core H10 from the WPWP were compared with various proxies of precipitation and were combined with elemental geochemistry and clay mineral assemblages to evaluate the main provenance, precipitation variability and orbital period characteristics of WPWP sediments since MIS8.

2 Study area

The study area is located at the junction of the Pacific, Philippine, and Caroline Plates, as well as the intersection of the Yap Trench, Western Caroline Ridge, and Sorol Trough (Figure 1). The area is geologically active and has a complex circulation system. The North Equatorial Current (NEC) in the northern part of the study area is one of the major sources of water in the tropical western Pacific and forms the Kuroshio Current (KC) to the north and Mindanao Current (MC) to the south, off the coast of the Philippines (Nitani, 1972). As the MC flows through the southern Philippines, a part of it flows eastward into the North Equatorial Countercurrent (NECC), while the other flows along the southern tip of Mindanao into the Celebes Sea (Wyrtki, 1961). The undercurrents include the North Equatorial Undercurrent (NEUC), Luzon Undercurrent (LUC), and Mindanao Undercurrent (MUC). The New Guinea Coastal Undercurrent (NGCUC), originating from the Antarctic Intermediate Water (AAIW), also flows northwest in this area (Tsuchiya, 1991). The South Equatorial Current flows into the WPWP primarily through the New Guinea Coastal Current (NGCC) and NGCUC (Peng et al., 2021). Northwest and southeast monsoons control the intensity and variation of the NGCC. However, the NGCUC is relatively stable (Fine et al., 1994). These ocean currents and water masses play important roles in the WPWP material inputs and water vapor transportation.

Previous studies of nearby areas suggest that the terrestrial material in the WPWP mainly came from New Guinea (Wu et al., 2013; Liu et al., 2018), situated in the southern part of the WPWP and is the largest island closest to the study area. New Guinea was formed by the island arc magmatism associated with plate subduction. New Guinea precipitation varies seasonally and regionally, and is affected by the monsoon, migrations of the ITCZ, and topography. Central New Guinea is mountainous, at an altitude of over 4,000 m with abundant rainfall and is the main

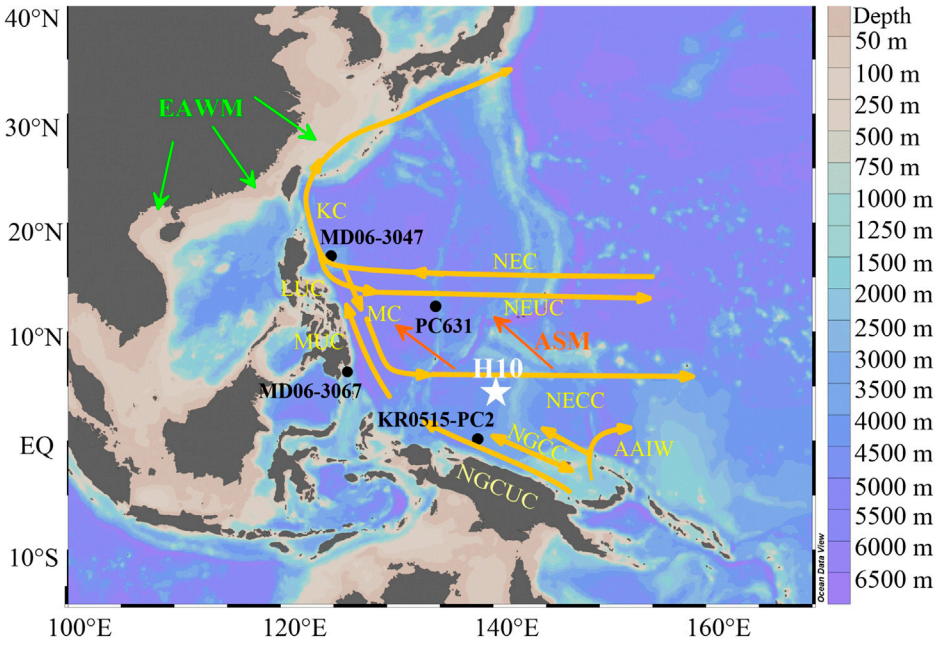

FIGURE 1
Geographical locations of core H10 (white pentagram). Black dots denote reference cores, including cores MD06-3047 (Xu et al., 2012), MD06-3067 (Kissel et al., 2010), PC631 (Seo et al., 2014), and KR0515-PC2 (Yamazaki and Horiuchi, 2016). The seabed topographic distribution was plotted using Ocean Data View software (Schlitzer, 2022). Orange arrows indicate the main oceanic currents acting in the WPWP region. AAIW, Antarctic Intermediate Water; KC, Kuroshio Current; LUC, Luzon Undercurrent; MC, Mindanao Current; MUC, Mindanao Undercurrent; NEC, North Equatorial Current; NECC, North Equatorial Counter Current; NEUC, North Equatorial Undercurrent; NGCC, New Guinea Coastal Current; NGCUC, New Guinea Coastal Undercurrent; EAWM, East Asian winter monsoon; ASM, Asian summer monsoon.

source of runoff. Subsequently, New Guinea has an annual river flow of 1.7×10^9 tons, even though its area is only 8×10^5 km^2 (Milliman, 1995).

The quantity of sediment transported from New Guinea to the deep-sea varies substantially owing to the gradient of the continental shelf, transportation route, and ocean current patterns (Walsh and Nittrouer, 2003). The northern continental shelf of New Guinea is narrow and steep, with an extremely low storage capacity. Thus, ~90% of the fluvial materials are transported to the deep-sea after passing through the continental slope (Kineke et al., 2000). Conversely, the southern continental shelf of New Guinea (part of the Gulf of Papua) is wide and flat; thus, most fluvial sediments cannot pass through it and are deposited at the estuary, with a minimal amount transported to the deep ocean (Walsh and Nittrouer, 2003). Therefore, high sediment transport from New Guinea may affect the material composition of sediments in the WPWP.

3 Materials and methods

3.1 Sample collection

The 310-cm H10 core sample (5°30.80′N, 139° 59.19′E, Figure 1) was collected from the southern margin of the WPWP at a depth of 3,790 m. The sediments in the study area are mainly clayey calcareous ooze with the largest number of calcareous organisms, followed by clay minerals and a small number of siliceous organisms. The core sediments were analyzed for major element concentrations, oxygen isotope ratios, clay mineral assemblage, and various magnetic parameters.

3.2 Method

3.2.1 Age establishment

Pulleniatina obliquiloculata (a planktonic foraminifera) from the H10 core was selected for oxygen isotope determination. A total of 150 oxygen isotope samples were tested in the whole column. First, each sample was soak in 5% hydrogen peroxide solution for 1 h to remove organic impurities, the grease on the shell surface was then washed with acetone solution, dried in an oven at 60 °C for 5 h, and transferred to a stable isotope mass spectrometer for testing at the State Key Laboratory of Marine Geology at Tongji University. The age of the H10 station was determined by comparing the δ^{18}O curve of *P. obliquiloculata* and the LR04 Stack δ^{18}O curve (the global standard oxygen isotope curve) (Lisiecki and Raymo, 2005) (Figure 2A).

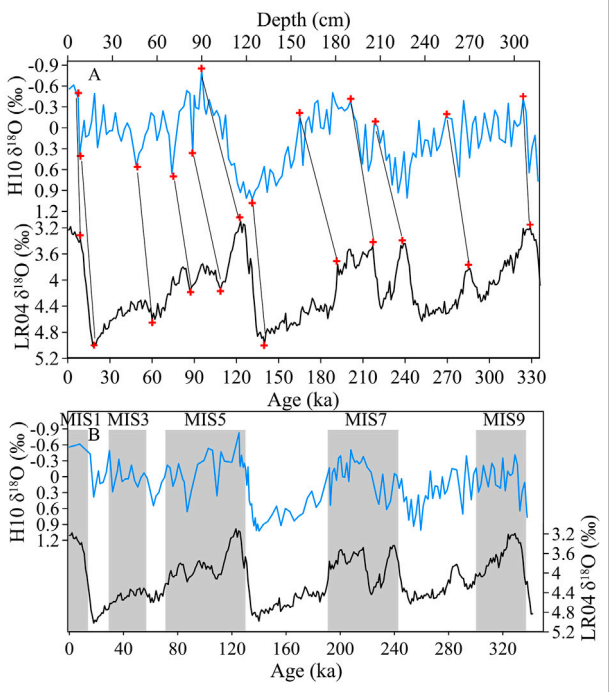

FIGURE 2
(A) Age control points (red cross symbol) of H10 $\delta^{18}O$ (compared with LR04 Stack $\delta^{18}O$ curve, Lisiecki and Raymo, 2005); and **(B)** age results.

TABLE 1 Age control points at different depths of the H10 station.

Depth (cm)	Age (kyr BP)	The state of LR04 $\delta^{18}O$
4	9	MIS1
8	18	MIS 2
46	62	MIS 4
70	87	MIS 5b
84	109	MIS 5d
90	123	MIS 5e
124	140	MIS 6
156	192	MIS 7
190	217	MIS7
206	240	MIS7
258	286	MIS8
306	329	MIS9

Significant peaks and valleys were selected as the age control points (Table 1) before linear interpolation was used to obtain the final age (Figure 2B). Comparison with the LR04 Stack $\delta^{18}O$ curve revealed that the H10 core contained sedimentary records since ~330 ka. To assess the changes of sediments in the equatorial western Pacific since MIS8, we selected samples within the depth of 280 cm for analysis.

3.2.2 Determination of the magnetic parameters

For pre-processing, samples were extracted at intervals of 2 cm and oven-dried at < 35°C. An agate mortar was used to powder the dried samples, which were then stored in sample bags. Approximately 1–2 g of each sample was wrapped in polyethylene plastic wrap and packed into a non-magnetic plastic box (2 × 2 × 2 cm^3). Another 0.2–0.3 g of each sample was stored in small non-magnetic capsules for subsequent analytical measurements.

The mass normalized magnetic susceptibility (χ) of the sediments was measured using the MFK1-FA rotating multi-frequency Kappabridge. The low- and high-frequency magnetic susceptibilities (χ_{lf} and χ_{hf}) were measured with frequencies of 967 and 15,616 Hz, respectively. The isothermal remanent magnetization (IRM) was measured with a 755-4KU Channel superconducting magnetometer and an ASC pulse magnetometer. The IRM component unmixing was performed using the web application MAX Unmix (Maxbauer et al., 2016). The SIRM was obtained by placing the samples in a 1 T (maximum) magnetic field and setting a 300-mT magnetic field in the opposite direction prior to conducting measurements to obtain the corresponding IRM_{-300mT}. The "hard" isothermal remanence magnetization (HIRM) was calculated using Eq. 1:

$$HIRM = (SIRM + IRM_{-300mT})/2 \quad (1)$$

All remanent measurements were conducted in a magnetically shielded room with an accuracy of $\times 110^{-12}$ Am^2.

Hysteresis loops and first-order reversal curves (FORCs) of the samples were measured using a VSM Model 8604 magnetometer system. The hysteresis loops were corrected to remove the influence of paramagnetic components and obtain the saturation magnetization (M_s), saturation remanence magnetization (M_{rs}), coercivity (B_c), and remanence coercivity (B_{cr}). All magnetic measurements above were conducted at the paleomagnetism laboratory of China University of Geosciences, Wuhan.

Temperature-dependent susceptibility (χ–T) curves of representative samples were measured using a MFK2-FA Kappabridge with CS-3 high-temperature furnace (AGICO), from 50°C to 700°C in an argon environment.

3.2.3 Elemental geochemistry

The samples were taken at 5 cm intervals then dried and ground before analysis. After weighing 0.05 g of each sample into a Teflon digestion tank, 3 ml of pure nitric acid and hydrofluoric acid (1:1) was added to each tank, the steel sleeve was stamped

and sealed, and the tank was placed in an oven at 190°C for 48 h. After cooling, the Teflon tank was placed on an electric hot plate, the samples were evaporated to a wet salt-like state, and 1 ml of nitric acid was added to the sample and evaporated (to remove residual hydrofluoric acid). Then, 3 ml of nitric acid (1:1) was added, the steel sleeve was stamped and sealed again, and the tank was placed in an oven at 150 °C for 24 h to ensure that the sample was extracted completely. After cooling, the extract was transferred to a clean PET (polyester) bottle and calibrated to 25.00 g with deionized water. The samples were stored at ~4°C until further analysis. The major element concentrations were determined using a desktop X-ray fluorescence spectrometer (XRF, SPECTRO XEPOS, Germany).

Carbonate content was determined using an automatic potentiometric titrator. Samples were taken at intervals of 5 cm; based on the volumetric method, excessive hydrochloric acid was added to the sediment sample. After full reaction, the excessive hydrochloric acid was titrated with sodium hydroxide reagent. Carbonate content in the sample was calculated using Eq. 2 (Sun, 2011):

$$W(\mathrm{CaCO_3}) = \left[(\mathrm{V_0} - \mathrm{V_1})_{c(\mathrm{NaOH})} \cdot \mathrm{F} \right] / m \times 100 \qquad (2)$$

3.2.4 Clay mineral analysis

Clay mineral studies were performed on a < 2-μm fraction of each sample, as previously described by Wan et al. (2007). All samples were separated based on Stoke's settling velocity principle after removal of carbonate and organic matter by adding 15 ml 15% H_2O_2 and 10 ml 25% acetic acid in 60°C water bath for 3 h. X-ray diffraction analysis was performed on oriented mounts with a D8 Advance diffractometer (in the Key Laboratory of Marine Geology and Environment, Institute of Oceanography, Chinese Academy of Sciences). Each sample was analyzed three times, including air drying, ethylene glycol solvation at 60 °C for 12 h, and heating at 550°C for 2 h. Three main groups, i.e., smectite (including mixed illite–smectite), illite, and kaolinite plus chlorite, were estimated by weighting integrated peak areas of basal reflections in the glycolated state, with empirical factors (Biscaye, 1965). Random samples were selected for scanning (after 2 h at 550°C) to identify the proportions of kaolinite and chlorite from the 3.58/3.54 A double peak areas (Ehrmann, 1998; Xu et al., 2012).

4 Results

4.1 Profiles of geochemical elements and magnetic parameters

Major oxides, including Al_2O_3 (average 3.97%), Fe_2O_3 (average 2.13%) and TiO_2 (average 0.21%) (Figures 3B–D), which are related to terrigenous clasts, were in good agreement with the changes in oxygen isotope concentrations (Figure 3A). Among them, Al_2O_3 and TiO_2 were more indicative of terrigenous origins (Murray, 1994). The $CaCO_3$ content in the study area varied from 53.96% to 85.28% (average 72.51%), and were inversely correlated with the terrestrial elements (Figure 3E). Thus, to exclude the influence of carbonate dilution, we used the method of Hounslow and Maher (1999) to correct the magnetic parameters and chemical elements, i.e., normalized by the mass of the non-carbonate content of the sample. The difference in the carbonate-free basis element concentrations (TiO_{2cfb}, Al_2O_{3cfb}, and Fe_2O_{3cfb} averaged 0.74%, 14.45%, 7.69%, respectively) remained almost the same as that before correction (the red curve in Figure 3). Ti was almost unaffected by diagenesis and relatively stable in most sedimentary environments; therefore, it reflected the terrigenous clastic input in deep-sea sediments (Goldberg and Arrhenius, 1958). The low values of TiO_{2cfb} concentration (average 0.74%) were mainly found in the MIS2, 4, 6, and 8 stages (cold periods), while the high values were mainly found in the MIS3 and 5 stages (warm periods). The changes in Fe_2O_{3cfb} concentration were consistent with TiO_{2cfb} concentration, which were lowest in the MIS6 stage, and peaked during early MIS8 stage. The variation range of Al_2O_{3cfb} concentration was small in the MIS1-5 stages, while that of the MIS6-8 stages was large. However, it was generally high in interglacial periods, and low in glacial periods.

Since magnetic parameters and chemical elements were tested at different intervals, the corrected magnetic data (χ_{cfb} and $SIRM_{cfb}$) were sparse, hence the data in Figure 3 are the results of linear interpolation at a 1-ka interval to observe detailed changes, with the overall trend being similar to the prior one (Figures 3F–H). The types, contents, and particle sizes of the magnetic minerals in the samples were reflected using χ and SIRM (Thompson and Oldfield, 1986; Oldfield, 1994). On the profile, χ_{cfb} of the H10 samples varied greatly with a minimum, maximum, and average values of 3.3×10^{-7}, 13.5×10^{-7}, and 6.78×10^{-7} m^3/kg, respectively (Figure 3F). The $SIRM_{cfb}$ distribution ranged from 7.9×10^{-3} to 19.07×10^{-3} Am^2/kg (average 11.91×10^{-3} Am^2/kg). The high $SIRM_{cfb}$ values indicate that the samples contained large amounts of ferromagnetic minerals.

4.2 Types of magnetic minerals

Obtained χ–T curves can provide information on the mineralogy and mineral transformation during the heating process (Dunlop and Özdemir, 1997). According to the measured χ–T curves (Figures 4A–D), χ increased rapidly with increasing temperature until ~320°C and decreased gradually thereafter, likely due to the transformation of maghemite to hematite. At about 580°C, χ decreased sharply due to the presence of magnetite (Evans and Heller, 2003). The cooling curves are all above the heating curves, likely due to the new strongly magnetic minerals generated during the heating process. For example, iron-bearing silicate minerals or clay minerals decompose at

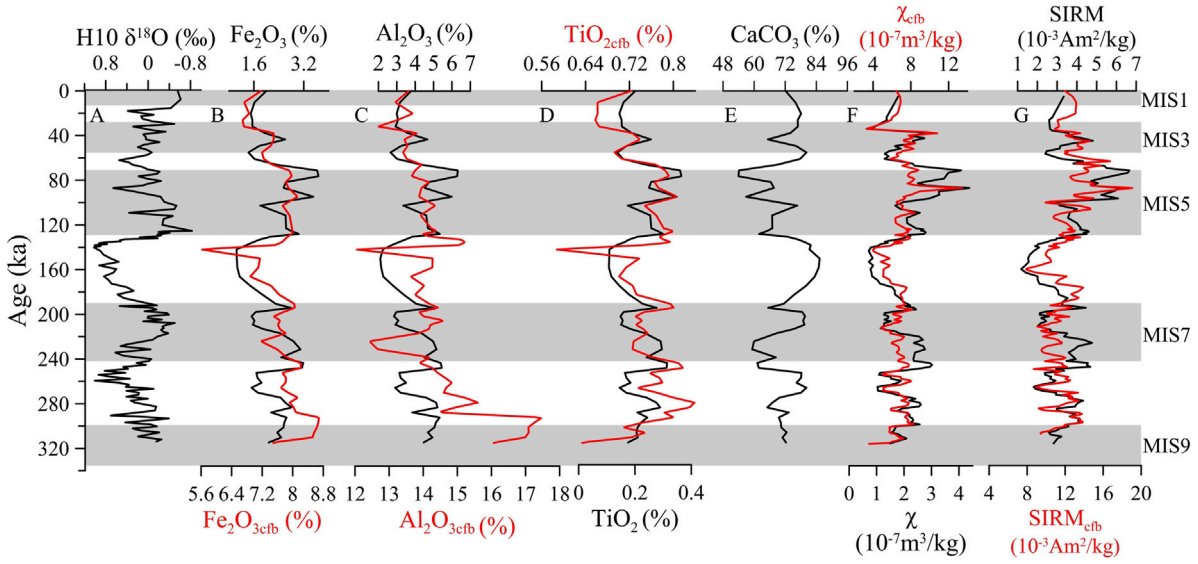

FIGURE 3
(A) Profiles of the $\delta^{18}O$; **(B)** Fe_2O_3 concentration and carbonate-free basis Fe_2O_3 (Fe_2O_{3cfb}); **(C)** Al_2O_3 concentration and carbonate-free basis Al_2O_3 (Al_2O_{3cfb}); **(D)** TiO_2 concentration and carbonate-free basis TiO_2 (TiO_{2cfb}); and **(F,G)** environmental magnetic parameters of the H10 core. Red curve represents the result of interpolation (linear interpolation at 1-ka intervals) using Matlab software.

high temperatures to form magnetite, while iron-bearing hydrate may also be transformed into magnetite (Dunlop and Özdemir, 1997; Hunt et al., 1995).

The saturation isothermal remanence acquisition curves and their reverse field demagnetization (RFD) curves were used to determine the types of magnetic minerals (Dankers, 1981). The five representative samples (Figure 5A) of these curves (Figure 5D) showed that the samples reached 70%–80% and >95% of saturation when the field strength was 100 and 300 mT, respectively. The magnetic coercivities of the RFD curves were 35–50 mT, indicating that the main magnetic carriers were low-coercivity magnetic minerals.

Morphological features of the hysteresis loops can reflect the types of magnetic minerals (Pike et al., 1999). Hysteresis loops of the samples formed closed curves when the magnetic field was ~200 mT (Figure 5B). Morphologically, the overall hysteresis loops were high and narrow, showing that the main magnetic minerals in the samples had low coercivities (predominantly magnetite). The types of magnetic minerals and state of magnetic domains of the samples could be determined based on the values of B_c (11.79–17.00 mT, averaging 14.85 mT) and B_{cr} (17.57–40.87 mT, averaging 29.46 mT). These were comparable to the theoretical values of 10 mT (B_c) and 33 mT (B_{cr}) for magnetite (Thompson and Oldfield, 1986).

MAX UnMix (Maxbauer et al., 2016) in the analysis of the magnetic components of IRM curves can be used to determine the contents of different components and the distribution range of coercivity. MAX UnMix results revealed the presence of four magnetic components in these representative samples (Figures 6A–E, Table 2). Component 1 (C1) of the five representative samples made a large contribution (97.6%–98.2%), with a low medium median acquisition field (B_h,18–41 mT) and a high dispersion parameter (DP) of 0.24–0.31. Component 2 (C2) had relatively low B_h (9.19–13.34 mT) and DP (0.16–0.29) values. Component 3 (C3) had a DP of 0.17–0.24 and a B_h of 96.60–137.71 mT for the five samples (Figure 6). The magnetic characteristics of hematite were identified only in component 4 (C4), but only for 6%–9%. The dispersion of the major component (C1) was wider than that of the common biogenic "hard" magnetite (DP generally <0.2) previously defined by Egli (2004) (supporting information are shown in Table 2 and Figure 6). This indicated that the magnetic minerals in H10 core are primarily of detrital magnetite, and possibly contain a small amount of biogenic magnetite (Heslop et al., 2002; Abrajevitch and Kodama, 2011; Roberts et al., 2011).

4.3 Magnetic domain states of the magnetic minerals

The FORCs were used to identify the types of magnetic minerals, magnetic domain states, and inter-particles interactions (Thompson and Oldfield, 1986). The horizontal axis represents the distribution characteristics of the coercivity of the magnetic minerals. The coercivity in the horizontal axes were between 10 and 40 mT (Figure 5C). This result was attributed to the soft ferromagnetic minerals. A narrow ridge was observed along the B_c axis at $B_u = 0$, indicating weak and negligible magnetostatic

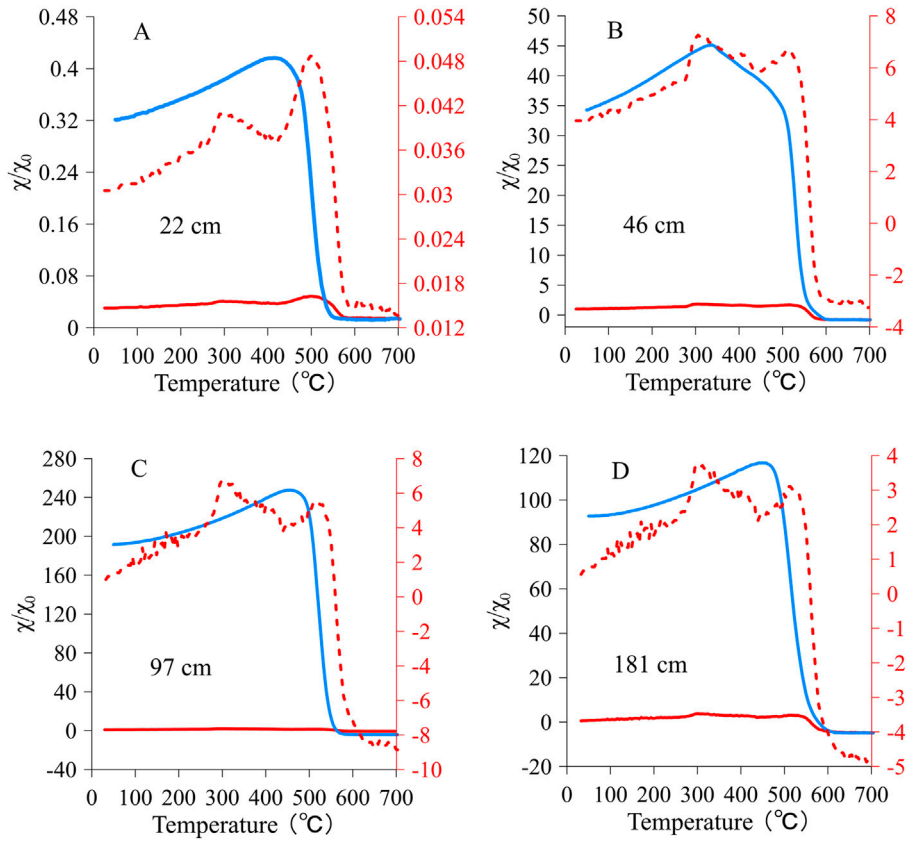

FIGURE 4
χ–T curves of representative core H10 samples. All χ values were normalized by χ values at room temperature. Red and blue lines correspond to the heating and cooling processes, respectively. **(A–D)** showed the results of representative samples at different depths.

interactions (Roberts et al., 2000; Yamazaki and Shimono, 2013). This central ridge is a distinctive feature of the biogenic magnetite (Roberts et al., 2011; Roberts et al., 2012; Yamazaki, 2012). The broad component had significant magnetostatic effects, which was in sharp contrast to the central ridge component representing biogenic magnetite; it was deduced that the magnetic minerals of the core were mainly terrigenous magnetite (Yamazaki, 2008, 2009), which is consistent with the results of IRM component unmixing analysis.

The Day diagram (Dunlop, 2002) is often used to determine the magnetic domain state of magnetic minerals. Most samples from the H10 core were concentrated in the PSD region (Figure 7), close to the SD area, which was consistent with the FORC results.

4.4 Composition characteristics of clay minerals

Regarding the studied core from the WPWP, the clay mineral assemblages mainly consisted of smectite (43%–68%, averaging 57%), illite (19%–37%, averaging 27%), kaolinite (2%–10%, averaging 6%) and chlorite (5%–16%, averaging 10%). The content of smectite was negatively correlated with those of the other three components (Figure 8). In addition, during transitions from glacial to interglacial periods, the content of smectite initially decreased sharply and subsequently increased. High smectite content was evident mainly in interglacial periods, while low smectite content was in glacial periods; the contents of the other minerals exhibited contrasting trends.

5 Discussion

5.1 Provenance of sediments

Various clay mineral assemblages in sediments are related to the rock type, climate, degree of physical and chemical weathering, and transportation process of the provenance area and can be used to track provenance changes (Liu et al., 2003; Wan et al., 2012; Yu et al., 2016). Numerous studies have shown that the adjacent continents are the provenance of oceanic clay

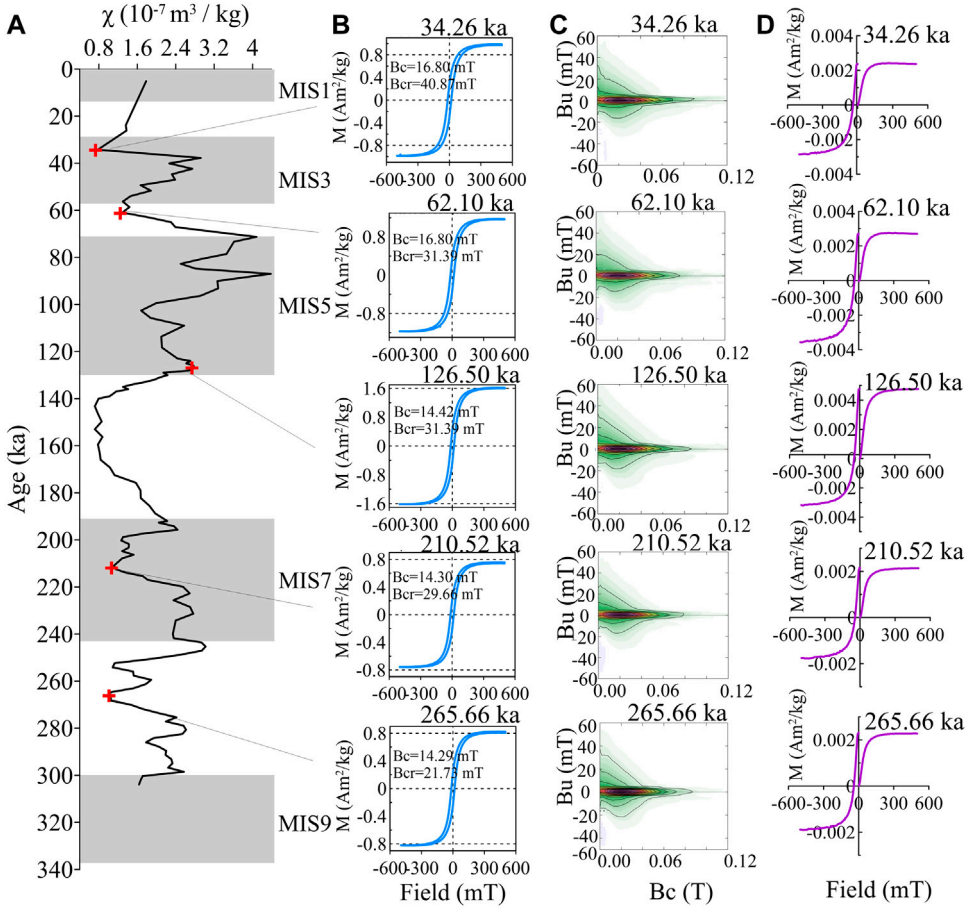

FIGURE 5
Rock magnetism results from the H10 core. **(A)** Variations in mass normalized magnetic susceptibility (χ); **(B)** hysteresis loops; **(C)** FORC plots; **(D)** IRM acquisition curves and RFD curves of representative samples.

minerals (Chamley, 1989). The continents undergo different degrees of chemical weathering due to different rock types and weathering conditions (Fagel, 2007). Generally, smectite and kaolinite are often formed in warm and humid environments with strongly chemical weathering, whereas illite and chlorite are formed under cold and arid conditions (Chamley, 1989).

Clay minerals of the H10 core were compared with those of various potential provenance areas (including Luzon Island, Palau Island, China's Loess Plateau, and New Guinea) to understand their provenance more accurately. A ternary diagram (Figure 9) comparative analysis showed that the H10 core contained smectite (average 57%), illite (average 27%), chlorite (average 10%), and kaolinite (average 6%). This clay mineral assemblage was intermediate between that of the Chinese Loess Plateau and Luzon Island, and closest to that of New Guinea. Illite is the main component of Quaternary loess (Shi et al., 2005), which has an extremely low smectite content. Therefore, the contribution of Asian aeolian dust (indicated by Chinese loess) to the clay minerals in the study area was insignificant.

The average contents of illite and chlorite in the core results near Luzon Island are 1% and 5%, respectively (Liu et al., 2009), greatly differing from our results. In addition, the clay mineral composition of Luzon during the glacial period was not significantly changed by the low paleo-temperature change. Therefore, the main source of illite in the sediments studied cannot be Luzon (Xu et al., 2012). Moreover, our magnetic parameters were consistent with the concentration trends of the terrestrial elements (Al_2O_3, TiO_2, and Fe_2O_3), suggesting that they are derived from the same terrigenous component. The iron-rich sediments in the equatorial western Pacific are mainly fluvial inputs from New Guinea, with negligible aeolian contribution (Wu et al., 2012, 2013). Therefore, we infer that

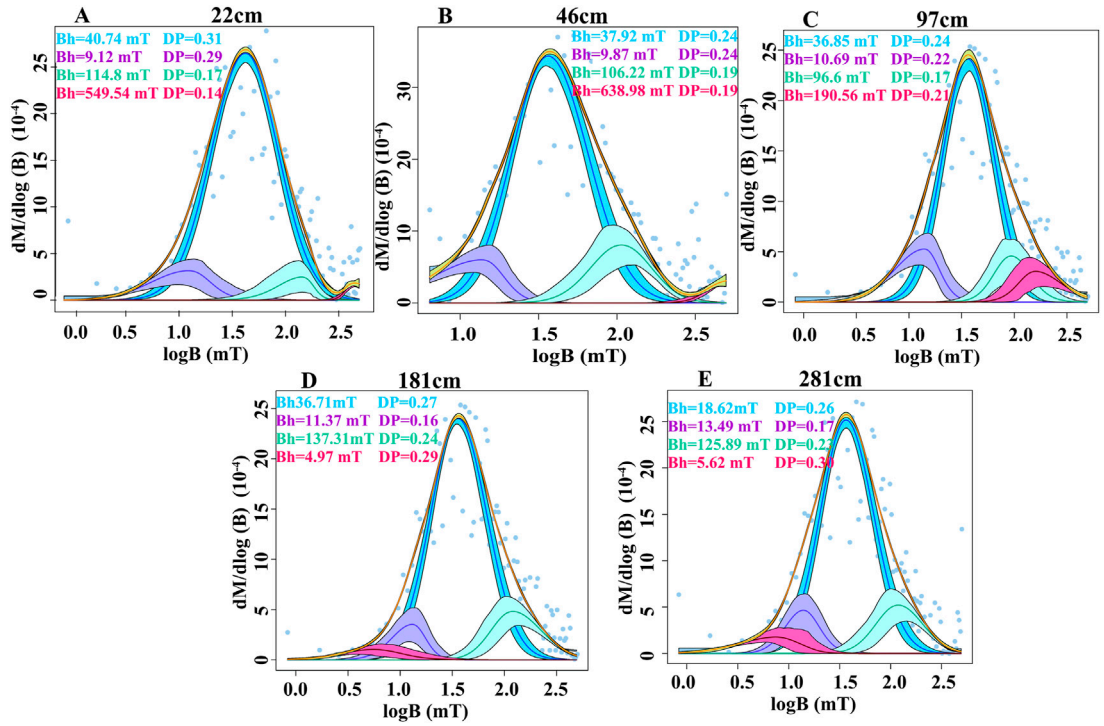

FIGURE 6
Unmixing of isothermal remanent magnetization (IRM) acquisition. **(A–E)** showed the results of representative samples at different depths.

TABLE 2 IRM component unmixing of representative samples.

Samples (cm)		22	46	97	181	281
Component						
C1	Bh (mT)	41.08	37.92	36.85	36.71	37.57
	DP	0.31	0.24	0.24	0.27	0.26
	P	0.98	0.98	0.98	0.98	0.98
C2	Bh (mT)	9.18	9.71	10.69	11.37	13.34
	DP	0.29	0.24	0.22	0.16	0.17
	p	0.12	0.17	0.21	0.16	0.18
C3	Bh (mT)	114.71	106.22	96.60	137.31	125.05
	DP	0.17	0.19	0.17	0.24	0.23
	p	0.09	0.23	0.19	0.20	0.21
C4	Bh (mT)	545.22	638.98	190.56	4.97	5.57
	DP	0.14	0.19	0.21	0.29	0.30
	p	0.06	0.09	0.13	0.04	0.07

B_h, mean remanence coercivity; DP, dispersion parameters; *p*, proportions.

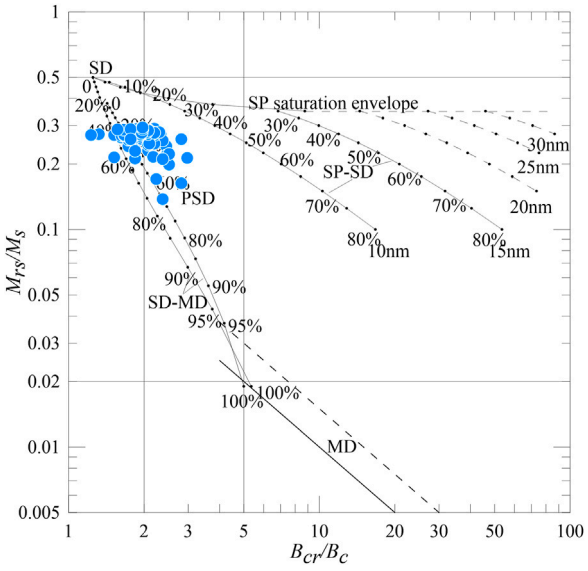

FIGURE 7
Day plot of hysteresis ratios for the samples of core H10. SD, single-domain; PSD, pseudo-single-domain; MD, multi-domain; SP, superparamagnetic (modified from Day et al., 1977; Dunlop, 2002).

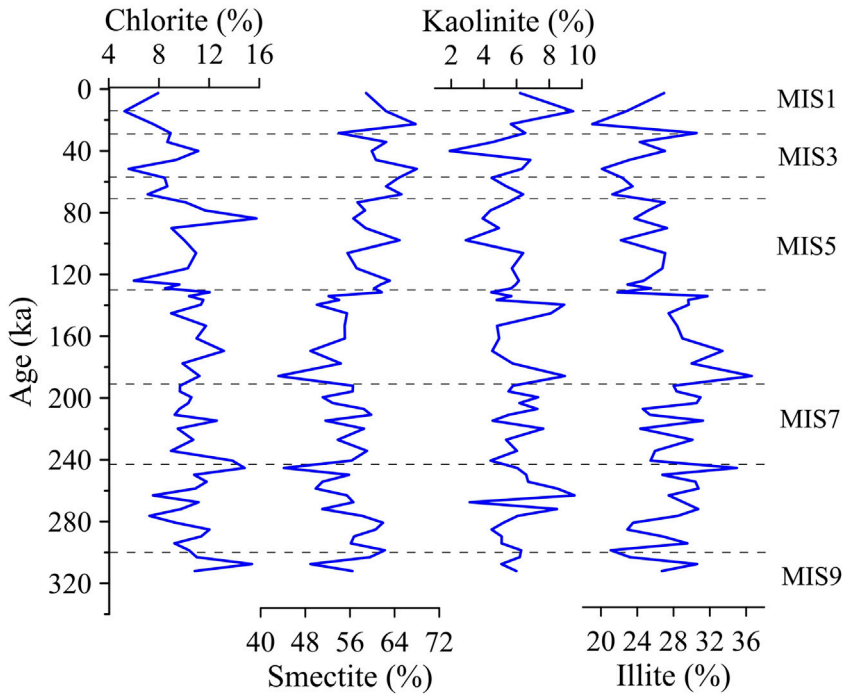

FIGURE 8
Relative contributions of the four major clay minerals to the clay fraction of sediments in core H10.

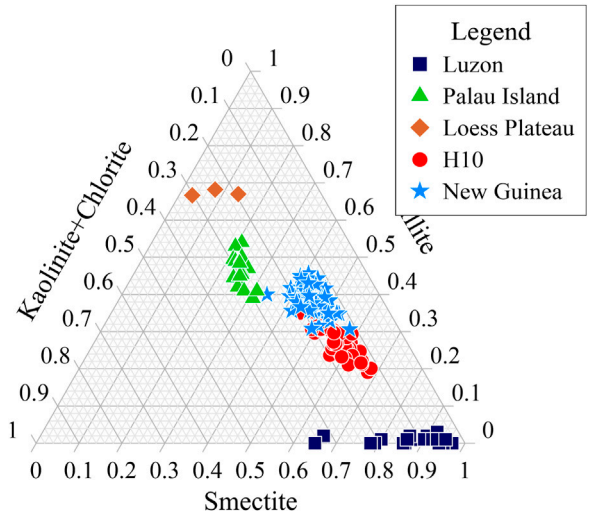

FIGURE 9
Ternary diagram of the clay mineralogy of core H10 sediments. Potential source areas: Luzon Island (Liu et al., 2009), Palau Island (Seo et al., 2014), China's Loess Plateau (Kalm et al., 1996; Shi et al., 2005), and New Guinea (Howell et al., 2014; Liu et al., 2018).

the provenance of the study area is mainly from New Guinea, with minimal contributions from Asia and Luzon Island, which confirms the conclusions of Wu et al. (2013) and Liu et al. (2018) indicating that terrigenous materials in the western equatorial Pacific sediments were predominantly derived from New Guinea.

The Western Caroline Basin is affected by western boundary currents, such as the NGCUC, which originates from the AAIW and strongly influences the sedimentation of the western Pacific (Yamazaki and Horiuchi, 2016). The NGCUC is the primary ocean current flowing into EUC (Wu et al., 2013). Therefore, the deposited magnetic minerals and terrigenous might be transported from New Guinea to the study area by NGCUC and NGCC (Tsuchiya, 1991; Wu et al., 2013; Peng et al., 2021).

5.2 Precipitation variations at the southern margin of the WPWP over the past 300 ka

Herein, we focus on common features supported by elemental records (TiO_{2cfb}) and magnetic parameters (χ_{cfb}, $SIRM_{cfb}$) of the H10 core to trace the precipitation variability at the southern margin of the WPWP, although these records can be affected by other factors, such as changes in ocean currents and sea level. First, previous studies suggested that the northern and southern parts of New Guinea had distinct source-to-sink patterns (Walsh and Nittrouer, 2003; Kineke et al., 2000). In high sea-level periods, most of the materials from the southern Fly River were deposited on the broad shelf and only a small amount was transported from the surface to the deep sea and into the subsurface current during the prevailing

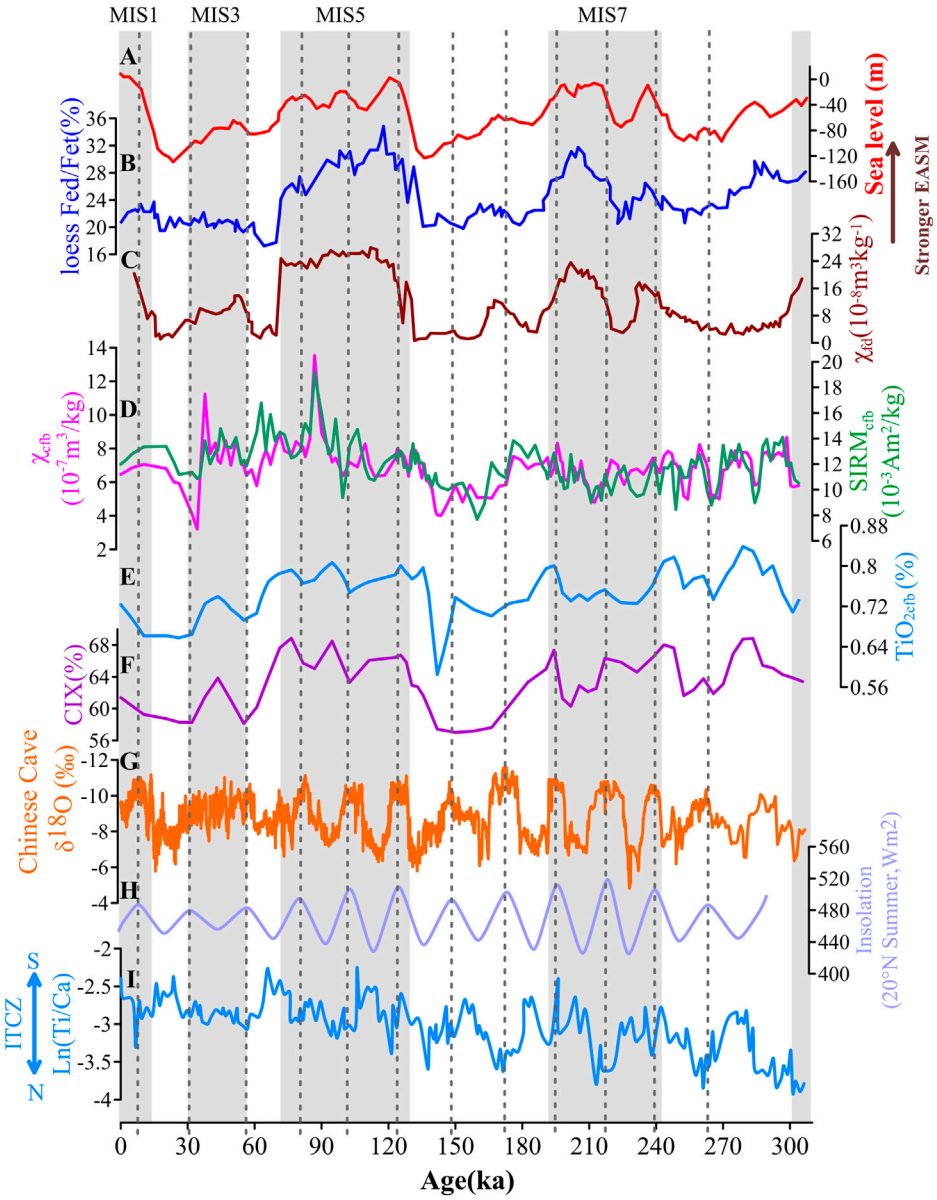

FIGURE 10
The variation of precipitation index of the H10 core over the past 300 ka. **(A)** Sea level (Spratt and Lisiecki, 2014); **(B)** Chemical weathering indicator F_{ed}/F_{et} of the Xifeng loess (Guo et al., 2000); **(C)** magnetic susceptibility frequency (χ_{fd}) records of the Luochuan loess (Hao et al., 2012); **(D)** carbonate-free basis χ (χ_{cfb}, magenta), carbonate-free basis SIRM ($SIRM_{cfb}$, gray); **(E)** carbonate-free basis TiO_2 (TiO_{2cfb}) of the H10 sediment; **(F)** CIA value of the H10 core sediment; **(G)** $\delta^{18}O$ sequence of stalagmites in the China's Sanbao Cave (Wang et al., 2008); **(H)** summer solar insolation at 20° N (Laskar et al., 2004); **(I)** the ln (Ti/Ca) indicator of ITCZ swing from the MD05-2920 core. Gray bars represent the interglacial periods, and gray broken lines indicate the maximum solar insolation periods.

northwestern monsoon (Milliman, 1995; Walsh and Nittrouer, 2003; Brunskill, 2004). However, in the narrow active continental margin, fluvial materials can directly cross the continental slope, carried by a high density turbidity current forced by gravity, and can even be transported by ocean currents for long distances without being controlled by sea-level changes (Figure 10A) (Brunskill, 2004). Fluvial materials from the Sepik River in the north are typically transported in this way (Milliman, 1995; Kineke et al., 2000; Brunskill, 2004; Kuehl et al., 2004). Overall, the impact of this mechanism on the study area is limited.

Second, NGCUC and NGCC in New Guinea, as the main route of AAIW to EUC, may affect the input of terrigenous materials to the ocean. Affected by the coastal monsoon, the NGCC flow velocity in the northwest direction increases during summer, while the flow velocity in the southeast direction increases during winter. Conversely, NGCUC is

relatively stable and flows northward continuously, but its velocity intensity is also affected by the coastal monsoon, which increases during summer and decreases during winter (Wyrtki, 1961). Therefore, monsoons may influence both precipitation and the strength of coastal currents in the region.

Magnetic parameters and terrestrial elements showed higher values during the interglacial periods compared with the glacial periods (Figure 3). Additionally, the amplitudes of their variations were the highest during the interglacial period. Therefore, we infer that the primary factor may be closely related to the summer monsoon. Previous studies have reported that magnetic susceptibility in loess-paleosol could be an indicator of the EASM (Deng, 2007; Nie et al., 2016). The magnetic susceptibility frequency (χ_{fd}) (Hao et al., 2012) and loess weathering index (F_{ed}/F_{et}) at the Xifeng (Guo et al., 2000) profile are also accepted as indicators of the EASM. Therefore, χ_{fd} and loess F_{ed}/F_{et} (Figures 10B,C) were selected for a comparison with our precipitation proxies (Figures 10D,E). The results show that the magnetic records of core H10 have similar changes with the EASM index (χ_{fd} and loess F_{ed}/F_{et}) in the long-time scale, showing high values in the interglacial period and low values in the glacial period. This suggests that the precipitation proxies of the equatorial western Pacific sediments are closely linked with the evolution of EASM.

Monsoon strength affects precipitation, which determines the degree of chemical weathering at the sediment provenance area. Elemental geochemical methods have been widely used in the evolution of Asian monsoon and Pacific Ocean sediments (Chen et al., 2018). The Chemical Index of Alteration that excludes CaO (CIX), as a common indicator to evaluate the chemical weathering intensity of the source region (Garzanti et al., 2014) and is defined as follows:

$$CIX = Al_2O_3 / (Al_2O_3 + Na_2O + K_2O) \times 100 \quad (3)$$

The CIX values of the core (Figure 10F), which ranged between 57.0 and 68.9 (average 63.1) regularly change. The high values occurred during the warm period, indicating enhanced chemical weathering and *vice versa*. The high χ_{cfb} and TiO_{2cfb} content represented great flux of terrigenous detritus—consistent with the high ratio of CIX—exhibiting the intensified erosion, and strong flux from river transport (Yang et al., 2016). Chemical weathering is closely related to the enhanced summer monsoon during the warm period, thus the increase in terrigenous debris flux suggests an enhanced summer monsoon.

The $\delta^{18}O$ of stalagmites in the Sanbao Cave, China (Figure 10G) records the precipitation variations of the EASM, which are closely related to summer solar insolation in the northern hemisphere (Cheng et al., 2017). Our precipitation proxies (Figures 10D,E) exhibited an inverse correlation with the northern hemisphere summer solar insolation (Figure 10H). With maximum summer solar insolation, our precipitation indicators showed minimum values. This relationship was particularly apparent in the MIS3, 5, and 8 periods. The variations of various parameters during interglacial periods are likely related to the variations of solar radiation. Figure 10H shows that the variations of solar radiation were also relatively large during interglacial periods. In this study area, considering the factors affecting paleo-precipitation changes in the southern margin of the WPWP, we believe that the inverse correlation between our precipitation proxies and the solar insolation in the northern hemisphere is due to the ITCZ migration. The precipitations for the northern continental and the southern ocean are in contrast as the increased solar insolation in the northern hemisphere moved the ITCZ northward (Igarashi and Oba, 2006; Tachikawa et al., 2014). The ln (Ti/Ca) index (Figure 10I) from sediments in northern New Guinea indicate oscillations in the ITCZ, with a southerly shift of the ITCZ corresponding to high values of our indices (χ_{cfb}, $SIRM_{cfb}$ and TiO_{2cfb}) and a northerly shift of the ITCZ corresponding to low values of those indices.

A similar pattern was recorded in the cores MD06-3067 (6°30.86′N, 126°29.86′E) and KR0515-PC2 (0°08.99′S, 138°56.97′E) (Kissel et al., 2010; Yamazaki and Horiuchi, 2016), which were attributed to the migration of the ITCZ, ocean currents, or monsoons. Other studies also proposed that the migration of ITCZ caused local precipitation changes (Wu et al., 2012).

There are two possible reasons why our precipitation index showed the opposite relationship with the EASM intensity recorded by loess and stalagmite. First, both the loess magnetic sensitivity index and stalagmite oxygen isotopes are widely recognized as EASM indicators. However, the former suggests that the EASM variability is dominated by the glacial–interglacial cycles (~100 ka), with the precession period being of minor importance; this is obviously different from that suggested by the stalagmite oxygen isotope sequence (Sun et al., 2006). Cheng et al. (2021) concluded that this difference is related to the variation of precipitation due to the precession cycles and the significant change of loess accumulation rate. In other words, the simple magnetic susceptibility index underestimates the precipitation changes due to the precession cycles, while the ASM is mainly driven by precession (Kong et al., 2020). Our magnetic parameters and geochemical element records are positively correlated with the loess index at the glacial–interglacial cycles; at the precession cycles, they are correlated with the stalagmite index, albeit exhibiting negative correlations. In brief, our sedimentary record is closely related to the summer monsoon. The two indicators exhibiting contrasting trends may be attributed to differences in resolution. Second, since New Guinea is the primary source area for the transport of terrestrial components to the study area, the precipitation and ocean current changes in New Guinea are controlled by the Australian monsoon, our precipitation records thus may be influenced by the Asia–Australia monsoon system, which is the manifestation of ITCZ migration. Therefore, we believe that the precipitation in the western equatorial Pacific is mainly affected by the movement of ITCZ and monsoon precipitation, which further affects the amount of provenance input in the study area.

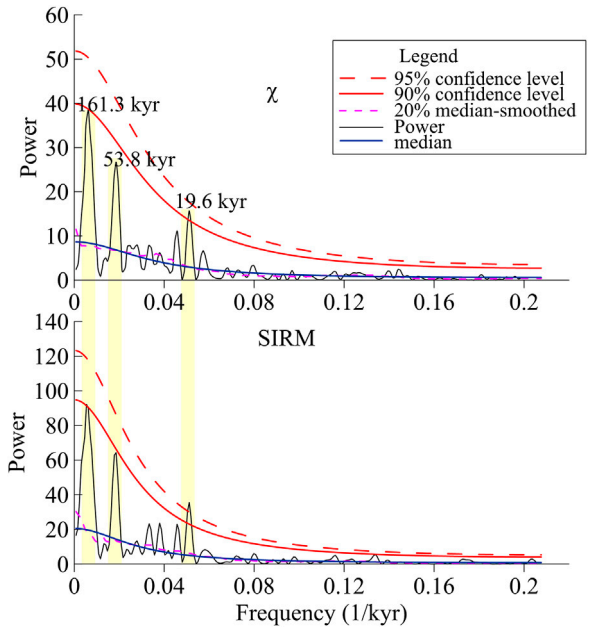

FIGURE 11
Time series analysis of χ and SIRM. They were interpolated to a median 0.2-m sample rate. Confidence levels in this study were determined following the robust noise modelling methods of Mann and Lees (1996).

The variation in the ITCZ shifting indicated by ln (Ti/Ca) exhibited a distinct precession cycle (Tachikawa et al., 2011). To extract the components of the orbital periods throughout the paleoenvironmental evolution, we used the Acycle 2.4.0 software (Li et al., 2016; Li et al., 2019) to perform Lomb–Scargle spectrum analysis (Lomb, 1976; Scargle, 1982) on χ and SIRM.

According to the energy spectrum results (Figure 11), both χ and SIRM exhibited significant precession periods of 19.6 ka in the high-frequency band, whereas poorly correlated (or non-existent) periods were found in the mid- and low-frequency bands. Among them, the 53.8 ka period in the mid-frequency band resulted from the combined effect of precession and inclination (Berger, 1977, 1978) and is considered to be a large-scale solar insolation event (Clemens et al., 1991). The 161.3 ka period in the low-frequency band was not evident. The 19.6 ka period in the high-frequency band demonstrated a high confidence level; therefore, we hypothesize that precession forcing controls the precipitation variability over the southern margin of the WPWP. After the χ and SIRM precession cycles were superimposed on the glacial–interglacial sequence, the concentrations of interglacial magnetic minerals and high contents of terrigenous assemblages corresponded to the strong summer monsoon and abundant precipitation in the southern margin of the WPWP. An energy spectrum analysis revealed a dominant precession period, in accordance with previous simulation results of the Milankovitch cycles at various latitudes. This precession period played a significant role in the low-latitude regions (Short et al., 1991). Therefore, we hypothesize that the precipitation change in the southern margin of the WPWP region is regulated by precession.

6 Conclusion

To investigate precipitation changes in the tropical western Pacific, we determined the chemical composition, clay mineral composition, and magnetic parameters of marine sediment core H10 since MIS8. Deposition in the equatorial western Pacific is associated with high terrigenous deposition rates and abundant year-round precipitation in the northern part of the neighboring island of New Guinea. Through a comparative analysis of the mineral assemblage characteristics of core H10 and the potential provenance area, it is concluded that the provenance of core H10 is mainly from the input of the coastal current of New Guinea.

The χ and SIRM indices of precipitation records are basically inversely correlated with the $\delta^{18}O$ records of stalagmites in Sanbao Cave, China—which represent the intensity of EASM—indicating a close relationship between the Australian monsoon and East Asian monsoon in the past four climate cycles. The precipitation records vary in phase with EASM on glacial-interglacial cycles, by in reverse phase during precessional cycles. It indicates that the precipitation changes in the western Pacific may be affected by both high and low latitudes, and the phase relationship with the EASM also differs at different time scales. The spectral analysis of χ and SIRM components showed that the precipitation in the western equatorial Pacific has a significant precession period, which further indicates that the interhemispheric orbital forcing is the dominant factor determining the precipitation in the western equatorial Pacific.

Data availability statement

The original contributions presented in the study are included in the article/Supplementary Material, further inquiries can be directed to the corresponding author.

Author contributions

GW: conceptualization, methodology, software, formal analysis, and writing (original draft preparation, and review and editing). JX: conceptualization, methodology, data curation, validation, formal analysis, investigation, resources, writing (review and editing), funding acquisition, project administration. ZJ: methodology, validation, formal analysis, resources, writing (review and editing). GL: resources, supervision. YZ: software, methodology. WZ: validation, funding acquisition, writing (review and editing). YL: investigation, software, visualization. All authors have read and agreed to the published version of the manuscript.

Funding

This research was funded by the Global Change and Air-Sea Interaction Project granted by the Ministry of Natural Resources of China (grant number GASI-02-PAC-CJ15) the National Natural Science Foundation of China (grants 42,103,027, 41,976,198, 42,274,089 and 91,858,203), and the Taishan Scholar grant to Guangxue Li.

Acknowledgments

The authors would like to thank the crew and scientists on the voyage of GASI-02-PAC-CJ15 cruise for sample collection.

Conflict of interest

The authors declare that the research was conducted in the absence of any commercial or financial relationships that could be construed as a potential conflict of interest.

Publisher's note

All claims expressed in this article are solely those of the authors and do not necessarily represent those of their affiliated organizations, or those of the publisher, the editors and the reviewers. Any product that may be evaluated in this article, or claim that may be made by its manufacturer, is not guaranteed or endorsed by the publisher.

Supplementary material

The Supplementary Material for this article can be found online at: https://www.frontiersin.org/articles/10.3389/feart.2022.1092686/full#supplementary-material

References

Abrajevitch, A., and Kodama, K. (2011). Diagenetic sensitivity of paleoenvironmental proxies: A rock magnetic study of Australian continental margin sediments. *Geochem., Geophys., Geosyst.* 12, Q05Z24. doi:10.1029/2010GC003481

An, Z., Liu, T., Lu, Y., Porter, S. C., Kukla, G., Wu, X., et al. (1990). The long-term paleomonsoon variation recorded by the loess-paleosol sequence in Central China. *Quat. Int.* 7–8, 91–95. doi:10.1016/1040-6182(90)90042-3

Beaufort, L., van der Kaars, S., Bassinot, F. C., and Moron, V. (2010). Past dynamics of the Australian monsoon: precession, phase and links to the global monsoon concept. *Clim. Past.* 6, 695–706. doi:10.5194/cp-6-695-2010

Berger, A. L. (1977). Support for the astronomical theory of climatic change. *Nature* 269, 44–45. doi:10.1038/269044a0

Berger, A. L. (1978). Long-term variations of daily insolation and quaternary climatic changes. *J. Atmos. Sci.* 35, 2362–2367.

Biscaye, P. E. (1965). Mineralogy and sedimentation of recent deep-sea clay in the Atlantic Ocean and adjacent seas and oceans. *Geol. Soc. Am. Bull.* 76, 803–832.

Brunskill, G. (2004). New Guinea and its coastal seas, a testable model of wet tropical coastal processes: An introduction to Project TROPICS. *Cont. Shelf Res.* 24, 2273–2295. doi:10.1016/j.csr.2004.08.001

Chamley, H. (1989). *Clay sedimentology*. Heidelberg: Springer Berlin, 623.

Chen, S., Qiao, P., Zhang, H., Xie, X., Cui, Y., and Shao, L. (2018). Geochemical characteristics of oligocene-miocene sediments from the deepwater area of the northern south China sea and their provenance implications. *Acta Oceanol. Sin.* 37, 35–43. doi:10.1007/s13131-017-1127-7

Cheng, H., Edwards, R. L., Sinha, A., Spötl, C., Yi, L., Chen, S., et al. (2017). Correction: Corrigendum: The Asian monsoon over the past 640, 000 years and ice age terminations. *Nature* 541, 122. doi:10.1038/nature20585

Cheng, H., Zhang, H., Cai, Y., Shi, Z., Yi, L., Deng, C., et al. (2021). Orbital-scale Asian summer monsoon variations: Paradox and exploration. *Sci. China Earth Sci.* 64, 529–544. doi:10.1007/s11430-020-9720-y

Clemens, S., Prell, W., Murray, D., Shimmield, G., and Weedon, G. (1991). Forcing mechanisms of the Indian Ocean monsoon. *Nature* 353, 720–725. doi:10.1038/353720a0

Dang, H., Jian, Z., Kissel, C., and Bassinot, F. (2015). Precessional changes in the Western equatorial pacific hydroclimate: A 240 kyr marine record from the halmahera sea, East Indonesia. *Geochem. Geophys. Geosyst.* 16, 148–164. doi:10.1002/2014GC005550

Dang, H., Wu, J., Xiong, Z., Qiao, P., Liu, T., and Jian, Z. (2020). Orbital and sea-level changes regulate the iron-associated sediment supplies from Papua New Guinea to the equatorial Pacific. *Quat. Sci. Rev.* 239, 106361. doi:10.1016/j.quascirev.2020.106361

Dankers, P. (1981). Relationship between median destructive field and remanent coercive forces for dispersed natural magnetite, titanomagnetite and hematite. *Geophys. J. R. Astron. Soc.* 64, 447–461. doi:10.1111/j.1365-246x.1981.tb02676.x

Day, R., Fuller, M., and Schmidt, V. A. (1977). Hysteresis properties of titanomagnetites: Grain-size and compositional dependence. *Phys. Earth Planet. Inter.* 13, 260–267. doi:10.1016/0031-9201(77)90108-x

Dean, W. E., Gardner, J. V., and Piper, D. Z. (1997). Inorganic geochemical indicators of glacial-interglacial changes in productivity and anoxia on the California continental margin. *Geochim. Cosmochim. Acta.* 61, 4507–4518. doi:10.1016/s0016-7037(97)00237-8

Deng, C., Mao, Y., Hu, F., and Zhang, X. (2007). Development of gas chromatography-mass spectrometry following microwave distillation and simultaneous headspace single-drop microextraction for fast determination of volatile fraction in Chinese herb. *Quat. Sci.* 2, 193–198. doi:10.1016/j.chroma.2006.08.074

Ding, Z., Liu, T.-s., Rutter, N. W., Yu, Z., Guo, Z., and Zhu, R. (1995). Ice-volume forcing of East Asian winter monsoon variations in the past 800, 000 years. *Quat. Res.* 44, 149–159. doi:10.1006/qres.1995.1059

Dunlop, D. J. (2002). Theory and application of the Day plot (M_{rs}/M_sversusH_{cr}/H_c) 1. Theoretical curves and tests using titanomagnetite data. *J. Geophys. Res. Solid Earth* 107, 2056. EPM 4–1–EPM 4–22. doi:10.1029/2001jb000486

Dunlop, D. J., and Özdemir, Ö. (1997). *Rock magnetism: Fundamentals and frontiers*. New York: Cambridge University Press

Egli, R. (2004). Characterization of individual rock magnetic components by analysis of remanence curves.: 2. Fundamental properties of coercivity distributions. *Phys. Chem. Earth, Parts A/B/C.* 29 (13–14), 851–867. doi:10.1016/s1474-7065(04)00129-9

Ehrmann, W. (1998). Implications of late eocene to early miocene clay mineral assemblages in McMurdo sound (ross sea, Antarctica) on paleoclimate and ice dynamics. *Palaeogeogr. Palaeoclimatol. Palaeoecol.* 139, 213–231. doi:10.1016/S0031-0182(97)00138-7

Evans, M. E., and Heller, F. (2003). *Environmental magnetism: Principles and applications of enviromagnetics*. San Diego, CA: Academic Press

Fagel, N. (2007). Chapter four clay minerals, deep circulation and climate. *Dev. Mar. Geol.* 1, 139–184. doi:10.1016/S1572-5480(07)01009-3

Fine, R. A., Lukas, R., Bingham, F. M., Warner, M. J., and Gammon, R. H. (1994). The western equatorial pacific: A water mass crossroads. *J. Geophys. Res.* 99, 25063–25080. doi:10.1029/94jc02277

Fraser, N., Kuhnt, W., Holbourn, A., Bolliet, T., Andersen, N., Blanz, T., et al. (2014). Precipitation variability within the West pacific warm pool over the past 120 ka: Evidence from the davao Gulf, southern Philippines. *Paleoceanography* 29, 1094–1110. doi:10.1002/2013PA002599

Gadgil, S. (2003). The Indian monsoon and its variability. *Annu. Rev. Earth Planet. Sci.* 31, 429–467. doi:10.1146/annurev.earth.31.100901.141251

Gao, Y., Fan, S. M., and Sarmiento, J. L. (2003). Aeolian iron input to the ocean through precipitation scavenging: A modeling perspective and its implication for natural iron fertilization in the ocean. *J. Geophys. Res. Atmos.* 108, 4221. doi:10.1029/2002JD002420

Garzanti, E., Vermeesch, P., Padoan, M., Resentini, A., Vezzoli, G., and Andò, S. (2014). Provenance of passive-margin sand (Southern Africa). *Geology* 122, 17–42. doi:10.1086/674803

Goldberg, E. D., and Arrhenius, G. (1958). Chemistry of Pacific pelagic sediments. *Geochim. Cosmochim. Acta.* 13, 153–212. doi:10.1016/0016-7037(58)90046-2

Guo, Z., Biscaye, P., Wei, L., Chen, X., Peng, S., and Liu, T. (2000). Summer monsoon variations over the last 1.2 Ma from the weathering of loess-soil sequences in China. *Geophys. Res. Lett.* 27, 1751–1754. doi:10.1029/1999gl008419

Han, J., Lü, H., Wu, N., and G, Z. (1996). The magnetic susceptibility of modern soils in China and its use for paleoclimate reconstruction. *Stud. Geophys. Geod.* 40, 262–275. doi:10.1007/BF02300742

Hao, Q., Wang, L., Oldfield, F., Peng, S., Qin, L., Song, Y., et al. (2012). Delayed build-up of Arctic ice sheets during 400, 000-year minima in insolation variability. *Nature* 490, 393–396. doi:10.1038/nature11493

Heslop, D., Dekkers, M. J., Kruiver, P. P., and van Oorschot, I. H. M. (2002). Analysis of isothermal remanent magnetization acquisition curves using the expectation-maximization algorithm. *Geophys. J. Int.* 148, 58–64. doi:10.1046/j.0956-540x.2001.01558.x

Hou, X., Xu, J., Jiang, Z., Cao, L., Zhang, Q., Li, G., et al. (2020). Response of environmental magnetic characteristics of sediments in the Western tropical Pacific to the East Asian Winter Monsoon. *Earth Sci. Front.*, 1–13. doi:10.13745/j.esf.sf.2020.5.55

Hounslow, W. H., and Maher, B. A. (1999). Source of the climate signal recorded by magnetic susceptibility variations in Indian Ocean sediments. *J. Geophys. Res. Solid Earth.* 104, 5047–5061. doi:10.1029/1998JB900085

Howell, A. L., Bentley, S. J., Xu, K., Ferrell, R. E., Muhammad, Z., and Septama, E. (2014). Fine sediment mineralogy as a tracer of latest Quaternary sediment delivery to a dynamic continental margin: Pandora Trough, Gulf of Papua, Papua New Guinea. *Mar. Geol.* 357, 108–122. doi:10.1016/j.margeo.2014.08.003

Hunt, C. P., Moskowitz, B. M., and Banerjee, S. K. (1995). "Magnetic properties of rocks and minerals," in *Rock physics & phase relations: A handbook of physical constants*. Washington, DC: American Geophysical Union 3, 189–204. doi:10.1029/RF003p0189

Igarashi, Y., and Oba, T. (2006). Fluctuations in the East Asian monsoon over the last 144ka in the northwest Pacific based on a high-resolution pollen analysis of IMAGES core MD01-2421. *Quat. Sci. Rev.* 25, 1447–1459.

Kalm, V. E., Rutter, N. W., and Rokosh, C. D. (1996). Clay minerals and their paleoenvironmental interpretation in the Baoji loess section, Southern Loess Plateau, China. *CATENA* 27, 49–61. doi:10.1016/0341-8162(96)00008-2

Kineke, G. C., Woolfe, K. J., Kuehl, S. A., Milliman, J. D., Dellapenna, T. M., and Purdon, R. G. (2000). Sediment export from the Sepik River, Papua New Guinea: Evidence for a divergent sediment plume. *Contin. Shelf Res.* 20, 2239–2266. doi:10.1016/s0278-4343(00)00069-8

Kissel, C., Laj, C., Kienast, M., Bolliet, T., Holbourn, A., Hill, P., et al. (2010). Monsoon variability and deep oceanic circulation in the Western equatorial pacific over the last climatic cycle: Insights from sedimentary magnetic properties and sortable silt. *Paleoceanography* 25 (3). doi:10.1029/2010PA001980

Kong, X., Zhou, W., Beck, J. W., Xian, F., Qiang, X., Ao, H., et al. (2020). Loess magnetic susceptibility flux: A new proxy of East Asian monsoon precipitation. *J. Asian Earth Sci.* 201, 104489. doi:10.1016/j.jseaes.2020.104489

Kuehl, S. A., Brunskill, G. J., Burns, K., Fugate, D., Kniskern, D., and Meneghini, L. (2004). Nature of sediment dispersal off the Sepik River, Papua New Guinea: preliminary sediment budget and implications for margin processes. *Cont. Shelf Res.* 24, 2417–2429. doi:10.1016/j.csr.2004.07.016

Kuroda, Y. (2000). Variability of currents off the northern coast of new Guinea. *J. Oceanogr.* 56, 103–116. doi:10.1023/A:1011122810354

Laskar, J., Robutel, P., Joutel, F., Gastineau, M., Correia, A. C. M., and Levrard, B. (2004). A long-term numerical solution for the insolation quantities of the Earth. *Astron. Astro Phys.* 428, 261–285. doi:10.1051/0004-6361:20041335

Li, M., Huang, C., Hinnov, L., Ogg, J., Chen, Z.-Q., and Zhang, Y. (2016). Obliquity-forced climate during the early triassic hothouse in China. *Geology* 44, 623–626. doi:10.1130/g37970.1

Li, M., Hinnov, L., and Kump, L. (2019). Acycle: Time-series analysis software for paleoclimate research and education. *Comput. Geosci.* 127, 12–22. doi:10.1016/j.cageo.2019.02.011

Lisiecki, L. E., and Raymo, M. E. (2005). A Pliocene-Pleistocene stack of 57 globally distributed benthic δ18O records. *Paleoceanography* 20. doi:10.1029/2004pa001071

Liu, Z., Trentesaux, A., Clemens, S. C., Colin, C., Wang, P., Huang, B., et al. (2003). Clay mineral assemblages in the northern South China Sea: Implications for East Asian monsoon evolution over the past 2 million years. *Mar. Geol.* 201, 133–146. doi:10.1016/S0025-3227(03)00213-5

Liu, Z., Zhao, Y., Colin, C., Siringan, F. P., and Wu, Q. (2009). Chemical weathering in Luzon, Philippines from clay mineralogy and major-element geochemistry of river sediments. *Appl. Geochem.* 24, 2195–2205. doi:10.1016/j.apgeochem.2009.09.025

Liu, J., Yan, W., Xu, W., and Zhong, L. (2018). Sediment provenance in the Western Pacific warm pool from the last glacial maximum to the early Holocene: Implications for ocean circulation and climatic change. *Palaeogeogr. Palaeoclimatol. Palaeoecol.* 493, 55–63. doi:10.1016/j.palaeo.2017.12.040

Lomb, N. R. (1976). Least-squares frequency analysis of unequally spaced data. *Astrophys. Space Sci.* 39, 447–462. doi:10.1007/bf00648343

Mann, M. E., and Lees, J. M. (1996). Robust estimation of background noise and signal detection in climatic time series. *Clim. Change* 33, 409–445. doi:10.1007/BF00142586

Maxbauer, D. P., Feinberg, J. M., and Fox, D. L. (2016). MAX Unmix: A web application for unmixing magnetic coercivity distributions. *Comput. Geosci.* 95, 140–145. doi:10.1016/j.cageo.2016.07.009

Meng, Q., Li, A., Li, T., and Jiang, F. (2009). "The magnetic properties of sediments from the West Philippine Sea and its paleoenvironmental significance," in AGU Fall Meet. Admin. (abstract id. GP43B-0852).

Milliman, J. D. (1995). Sediment discharge to the ocean from small mountainous rivers: The New Guinea example. *Geo-Marine Lett.* 15, 127–133. doi:10.1007/BF01204453

Murray, R. W. (1994). Chemical criteria to identify the depositional environment of chert: General principles and applications. *Sediment. Geol.* 90, 213–232. doi:10.1016/0037-0738(94)90039-6

Nie, J., Song, Y., and King, J. W. (2016). A review of recent advances in red-clay environmental magnetism and paleoclimate history on the Chinese Loess Plateau. *Front. Earth Sci.* 4, 27–29. doi:10.3389/feart.2016.00027

Nitani, H. (1972). "Beginning of the Kuroshio," in *Kuroshio: Physical aspects of the Japan current*. Editors H. Stommel and K. Yoshida (Seattle: University of Washingtonn Press), 129–163.

Okubo, S., and Takeuchi, H. (1979). Time series analysis of natural remanent magnetization in deep-sea sediments. *Geophys. J. Int.* 56, 309–318. doi:10.1111/j.1365-246x.1979.tb00166.x

Oldfield, F. (1994). Toward the discrimination of fine-grained ferrimagnets by magnetic measurements in lake and near-shore marine sediments. *J. Geophys. Res.* 99, 9045–9050. doi:10.1029/93JB03137

Peng, N., Dang, H., Wu, J., Aiello, I. W., and Jian, Z. (2021). Tectonic and climatic controls on the Plio-Pleistocene evolution of sediment discharge from Papua New Guinea. *Mar. Geol.* 441, 106627. doi:10.1016/j.margeo.2021.106627

Pike, C. R., Roberts, A. P., and Verosub, K. L. (1999). Characterizing interactions in fine magnetic particle systems using first order reversal curves. *J. Appl. Phys.* 85, 6660–6667. doi:10.1063/1.370176

Rao, Z., Liu, X., Hua, H., Gao, Y., and Chen, F. (2015). Evolving history of the East Asian summer monsoon intensity during the MIS5: Inconsistent records from Chinese stalagmites and loess deposits. *Environ. Earth Sci.* 73, 3937–3950. doi:10.1007/s12665-014-3681-z

Roberts, A. P., Pike, C. R., and Verosub, K. L. (2000). First-order reversal curve diagrams: A new tool for characterizing the magnetic properties of natural samples. *J. Geophys. Res.* 105, 28461–28475. doi:10.1029/2000jb900326

Roberts, A. P., Florindo, F., Villa, G., Chang, L., Jovane, L., Bohaty, S. M., et al. (2011). Magnetotactic bacterial abundance in pelagic marine environments is limited by organic carbon flux and availability of dissolved iron. *Earth Planet. Sci. Lett.* 310, 441–452. doi:10.1016/j.epsl.2011.08.011

Roberts, A. P., Chang, L., Heslop, D., Florindo, F., and Larrasoaña, J. C. (2012). Searching for single domain magnetite in the "pseudo-single-domain" sedimentary haystack: Implications of biogenic magnetite preservation for sediment magnetism and relative paleointensity determinations. *J. Geophys. Res.* 117 (B8). doi:10.1029/2012JB009412

Rodríguez-Tovar, F. J., Löwemark, L., and Pardo-Igúzquiza, E. (2011). Zoophycos cyclicity during the last 425ka in the northeastern South China Sea: Evidence for monsoon fluctuation at the Milankovitch scale. *Palaeogeogr. Palaeoclimatol. Palaeoecol.* 305, 256–263. doi:10.1016/j.palaeo.2011.03.006

Ruddiman, W. F. (2006). Orbital changes and climate. *Quat. Sci. Rev.* 25, 3092–3112. doi:10.1016/j.quascirev.2006.09.001

Scargle, J. D. (1982). Studies in astronomical time series analysis. II – statistical aspects of spectral analysis of unevenly spaced data. *Astrophys. J.* 263, 835. doi:10.1086/160554

Schlitzer, R. (2022). *Ocean data View*, 4. Available at: https://odv.awi.de/ (Accessed June 20, 2022).

Seo, I., Lee, Y. I., Yoo, C. M., Kim, H. J., and Hyeong, K. (2014). Sr-Nd isotope composition and clay mineral assemblages in eolian dust from the central Philippine Sea over the last 600 kyr: Implications for the transport mechanism of Asian dust. *J. Geophys. Res. Atmos.* 119 (11), 11, 492–511, 504. doi:10.1002/2014JD022025

Shang, S., Yang, X., Zhang, E., Wei, R., Tingwei, Z., and Zhou, Q. (2022). Variation in humidity and the forcing mechanism in Asian monsoon-influenced regions indicated by hematite/goethite from Baxian Lake, southern China, since AD 800. *Holocene* 32, 977–990. doi:10.1177/09596836221101250

Shi, Y. X., Dai, X. R., Song, Z. G., Zhang, W. G., and Wang, L. Q. (2005). Characteristics of clay mineral assemblages and their spatial distribution of Chinese loess in different climatic zones. *Acta Sedimentol. Sin.* 23, 690–695.

Short, D. A., Mengel, J. G., Crowley, T. J., Hyde, W. T., and North, G. R. (1991). Filtering of Milankovitch cycles by Earth's geography. *Quat. Res.* 35, 157–173. doi:10.1016/0033-5894(91)90064-C

Spratt, R. M., and Lisiecki, L. (2014). A Late Pleistocene sea level stack. *Clim. Past Discuss.* 12, 1079–1092. doi:10.5194/CP-12-1079-2016

Sun, Y. B., Clemens, S. C., An, Z. S., and Yu, Z. (2006). Astronomical timescale and palaeoclimatic implication of stacked 3.6-Myr monsoon records from the Chinese Loess Plateau. *Quat. Sci. Rev.* 25, 33–48. doi:10.1016/j.quascirev.2005.07.005

Sun, H. J. (2011). *Research of the paleoceanography of the Western Philippine Sea over the past 2.36Ma*. PhD dissertation. China: University of Chinese Academy of Sciences (Institute of Oceanology, CAS).

Tachikawa, K., Cartapanis, O., Vidal, L., Beaufort, L., Barlyaeva, T., and Bard, E. (2011). The precession phase of hydrological variability in the Western Pacific Warm Pool during the past 400 ka. *Quat. Sci. Rev.* 30, 3716–3727. doi:10.1016/j.quascirev.2011.09.016

Tachikawa, K., Timmermann, A., Vidal, L., Sonzogni, C., and Timm, O. E. (2014). CO2 radiative forcing and Intertropical Convergence Zone influences on Western Pacific warm pool climate over the past 400 ka. *Quat. Sci. Rev.* 86, 24–34. doi:10.1016/j.quascirev.2013.12.018

Thompson, R., and Oldfield, F. (1986). *Environmental magnetism*. London: Allen & Unwin, 1–52.

Trenberth, K. E., Stepaniak, D. P., and Caron, J. M. (2000). The global monsoon as seen through the divergent atmospheric circulation. *J. Clim.* 13, 3969–3993. doi:10.1175/1520-0442(2000)013%3C3969:TGMAST%3E2.0.CO;2

Tsuchiya, M. (1991). Flow path of the antarctic intermediate water in the Western equatorial south Pacific ocean. *Deep Sea Res. A* 38, S273–S279. doi:10.1016/S0198-0149(12)80013-6

Verosub, K. L., and Roberts, A. P. (1995). Environmental magnetism: Past, present, and future. *J. Geophys. Res.* 100, 2175–2192. doi:10.1029/94jb02713

Walsh, J. P., and Nittrouer, C. A. (2003). Contrasting styles of off-shelf sediment accumulation in New Guinea. *Mar. Geol.* 196, 105–125. doi:10.1016/S0025-3227(03)00069-0

Wan, S., Li, A., Clift, P. D., and Stuut, J.-B. W. (2007). Development of the East Asian monsoon: Mineralogical and sedimentologic records in the northern south China sea since 20 ma. *Palaeogeogr. Palaeoclimatol. Palaeoecol.* 254, 561–582. doi:10.1016/j.palaeo.2007.07.009

Wan, S., Yu, Z., Clift, P. D., Sun, H., Li, A., and Li, T. (2012). History of Asian eolian input to the West Philippine Sea over the last one million years. *Palaeogeogr. Palaeoclimatol. Palaeoecol.* 326-328, 152–159. doi:10.1016/j.palaeo.2012.02.015

Wang, H., and Mehta, V. M. (2008). Decadal variability of the Indo-Pacific warm pool and its association with atmospheric and oceanic variability in the NCEP-NCAR and soda reanalyses. *J. Clim.* 21, 5545–5565. doi:10.1175/2008jcli2049.1

Wang, Y., Cheng, H., Edwards, R. L., Kong, X., Shao, X., Chen, S., et al. (2008). Millennial- and orbital-scale changes in the East Asian monsoon over the past 224, 000 years. *Nature* 451, 1090–1093. doi:10.1038/nature06692

Wang, P. (2009). Global monsoon in a geological perspective. *Sci. Bull.* 54, 1113–1136. doi:10.1007/s11434-009-0169-4

Webster, P. J. (1994). The role of hydrological processes in ocean-atmosphere interactions. *Rev. Geophys. Rev. Geophys.* 32, 427–476. doi:10.1029/94rg01873

Wu, J., Liu, Z., and Zhou, C. (2012). Late Quaternary glacial cycle and precessional period of clay mineral assemblages in the Western Pacific warm pool. *Chin. Sci. Bull.* 57, 3748–3760. doi:10.1007/s11434-012-5277-x

Wu, J., Liu, Z., and Zhou, C. (2013). Provenance and supply of Fe-enriched terrigenous sediments in the Western equatorial Pacific and their relation to precipitation variations during the late Quaternary. *Glob. Planet. Change.* 108, 56–71. doi:10.1016/j.gloplacha.2013.06.002

Wyrtki, K. (1961). Physical oceanography of the southeast asian waters. *Naga Rep.* 2, 15.

Xu, Z., Li, T., Wan, S., Nan, Q., Li, A., Chang, F., et al. (2012). Evolution of East Asian monsoon: Clay mineral evidence in the Western Philippine Sea over the past 700kyr. *J. Asian Earth Sci.* 60, 188–196. doi:10.1016/j.jseaes.2012.08.018

Yamazaki, T., and Horiuchi, K. (2016). Precessional control on ocean productivity in the Western Pacific Warm Pool for the last 400 kyr: Insight from biogenic magnetite. *Geochem. Geophys. Geosyst.* 17, 4399–4412. doi:10.1002/2016gc006446

Yamazaki, T., and Shimono, T. (2013). Abundant bacterial magnetite occurrence in oxic red clay. *Geology* 41, 1191–1194. doi:10.1130/g34782.1

Yamazaki, T. (2008). Magnetostatic interactions in deep-sea sediments inferred from first-order reversal curve diagrams: Implications for relative paleointensity normalization. *Geochem. Geophys. Geosyst.* 9. doi:10.1029/2007GC001797

Yamazaki, T. (2009). Environmental magnetism of pleistocene sediments in the North pacific and ontong-java plateau: Temporal variations of detrital and biogenic components. *Geochem. Geophys. Geosyst.* 10. doi:10.1029/2009GC002413

Yamazaki, T. (2012). Paleoposition of the Intertropical Convergence Zone in the eastern Pacific inferred from glacial-interglacial changes in terrigenous and biogenic magnetic mineral fractions. *Geology* 40, 151–154. doi:10.1130/G32646.1

Yan, X. H., Ho, C. R., Zheng, Q., and Klemas, V. (1992). Temperature and size variabilities of the Western Pacific warm pool. *Science* 258, 1643–1645. doi:10.1126/science.258.5088.1643

Yang, X., Grapes, R., Zhou, H., and Yang, J. (2008). Magnetic properties of sediments from the pearl river delta, south China: Paleoenvironmental implications. *Sci. China Ser. D Earth Sci.* 51, 56–66. doi:10.1007/s11430-007-0151-4

Yang, X., Peng, X., Qiang, X., Li, N., Zhou, Q., and Wang, Y. (2016). Chemical weathering intensity and terrigenous flux in south China during the last 90, 000 Years—evidence from magnetic signals in marine sediments. *Front. Earth Sci.* 4. doi:10.3389/feart.2016.00047

Yu, Z., Wan, S., Colin, C., Yan, H., Bonneau, L., Liu, Z., et al. (2016). Co-evolution of monsoonal precipitation in East Asia and the tropical Pacific ENSO system since 2.36 Ma: New insights from high-resolution clay mineral records in the West Philippine Sea. *Earth Planet. Sci. Lett.* 446, 45–55. doi:10.1016/j.epsl.2016.04.022

Yuan, D., Cheng, H., Edwards, R. L., Dykoski, C. A., Kelly, M. J., Zhang, M., et al. (2004). Timing, duration, and transitions of the last interglacial Asian monsoon. *Science* 304, 575–578. doi:10.1126/science.1091220